Energy & Environmental Science

COMMUNICATION

View Article Online
View Journal | View Issue

Cite this: *Energy Environ. Sci.*, 2015, **8**, 552

Received 18th November 2014
Accepted 16th December 2014

DOI: 10.1039/c4ee03642e

www.rsc.org/ees

A silole copolymer containing a ladder-type heptacylic arene and naphthobisoxadiazole moieties for highly efficient polymer solar cells†

Zhiyun Zhang,‡[a] Francis Lin,‡[a] Hsieh-Chih Chen,*[ab] Hung-Chin Wu,[c] Chin-Lung Chung,[a] Chien Lu,[c] Shih-Hung Liu,[a] Shih-Huang Tung,[d] Wen-Chang Chen,[c] Ken-Tsung Wong*[a] and Pi-Tai Chou*[a]

We report a combination of a silole containing ladder-type heptacylic arene and naphthobisoxadiazole moieties for highly efficient polymer solar cells. This new class of PSiNO polymer possesses a planar, rigid backbone and a low-ordering framework. This unique feature facilitates chain extension, leading to high hole mobility and hence a high PCE of 8.37% without further thermal annealing.

The discovery of polymer-based bulk heterojunction (BHJ) structures has aided the development of high efficiency polymer solar cells (PSCs). In BHJ structures, a polymer donor and a fullerene acceptor are cast from a common solution to form a bicontinuous interpenetrating network for efficient exciton diffusion, charge separation and charge transport. Combining electron-rich and electron-deficient moieties to form donor–acceptor (D–A) copolymers has become a widely accepted strategy for designing low bandgap polymers. This is mainly due to the facile tunability of their electronic structure *via* controlling the intramolecular charge transfer (ICT) from donor to acceptor moieties.[1–10] In addition, vast numbers of studies about developing new photoactive materials, especially electron donating polymers[1–10] and innovations in device architecture,[11–16] have significantly increased power conversion efficiencies (PCEs), and PCEs of 8–9% for single-junction cells have been achieved.[3–6,10,12–15] In addition, there has also been significant research into developing inverted device structures, in which the charge collection of the electrode is opposite to that of conventional configurations, to enhance the performance of solar cells and device air-stability.[17,18] This technique is useful because of its favorable vertical phase separation and concentration gradient in the active layer.[19] Recently, incorporation of interfacial dipole layers for inverted PSCs has received much attention, because they can increase the internal built-in potential, decrease resistance, and improve the charge extraction and collection. Dipole layers modify the Fermi level alignment to either $E_{F,h}$ of the donor material or $E_{F,e}$ of the acceptor material for hole and electron transport toward the corresponding electrodes.[14,17,20] Consequently, both interfacial contact resistance and undesired charge recombination are minimized, enhancing the device performance.[21] Although this efficiency still lags behind silicon-based inorganic devices, the design and syntheses of various polymers are versatile and there is much scope for further improvement.

Broader context

Donor–acceptor (D–A) copolymers based on benzo[1,2-*b*:4,5-*b*′]-dithiophene (BDT) and dithieno[3,2-*b*:2′,3′-*d*]silole (DTS) show broad absorption, low-lying HOMO energy levels and high hole mobility. Therefore, BDT and DTS are attractive building blocks for highly efficient conjugated polymers. This inspired us to hybridize BDT/DTS units into mutually fused structures to increase planarity and charge transport efficiency, which could allow us to tune their optoelectronic properties and improve their photovoltaic performance. In this study, we report a straightforward synthetic method for preparing a series of low bandgap ladder-type D–A alternating copolymers that are highly rigid and coplanar. The polymers contain a seven-ring heptacyclic arene (ARSi) as the donor unit, and a dually-fused NO ring or nonfused BO ring as the acceptor moieties. Both polymers show low-lying HOMO energy levels that lead to high open-circuit voltages in the solar cell devices. The strong electron-withdrawing ability of NO moiety increases the absorption intensity, extends the absorption spectra toward the near IR region, and lowers the HOMO and LUMO energy levels and optical bandgap. Most significantly, the BHJ inverted device based on the PSiNO:$PC_{71}BM$ blend achieved a high PCE of 8.37% without thermal annealing, demonstrating PSiNO is a promising semiconducting polymer for high-performance photovoltaics.

[a]*Department of Chemistry, Center of Emerging Material and Advanced Devices, National Taiwan University, Taipei 106, Taiwan. E-mail: kenwong@ntu.edu.tw; chop@ntu.edu.tw*

[b]*Research Center for New Generation Photovoltaics, Graduate Institute of Energy Engineering, National Central University, Jhongli, 320, Taiwan. E-mail: austinchen@ncu.edu.tw*

[c]*Department of Chemical Engineering, National Taiwan University, Taipei 106, Taiwan*

[d]*Institute of Polymer Science and Engineering, National Taiwan University, Taipei 106, Taiwan*

† Electronic supplementary information (ESI) available. See DOI: 10.1039/c4ee03642e

‡ These authors contributed equally to this work.

A key target for organic–electronic materials is the extended π-conjugation of ladder-type polymers with coplanar geometry and their structural rigidification by covalently bonding adjacent aromatic units in the polymer backbone. In this framework, the π-system planarization facilitates π-electron delocalization that narrows the bandgap, and also suppresses rotational disorder about single bonds to reduce Marcus reorganization energies. Both these effects make exciton separation into free charge carriers facile.[22–25] For this approach, benzo[1,2-*b*:4,5-*b*′]-dithiophene (BDT) and dithieno[3,2-*b*:2′,3′-*d*]silole (DTS) are attractive as donor units because of their good electron-donating ability, planar molecular structure and fine-tuning through structural modifications.[2,4,5,8–10,26–28] D–A copolymers based on BDT or DTS show broad absorption, low-lying HOMO energy levels and high hole mobility,[2,4,5,8–10,26–28] indicating that BDT and DTS are good building blocks for highly efficient conjugated polymers. These results inspired us to hybridize BDT/DTS units into mutually fused structures to promote planarity and charge transport efficiency, which could allow us to tune their optoelectronic properties and improve their photovoltaic performance.

In this communication, we report a straightforward synthetic method for preparing a series of D–A alternating copolymers (Scheme 1) and their application to PSCs. The ladder-type 5,11-dihexyl-4,4,10,10-tetraoctylbenzo[1,2-*b*:4,5-*b*′]bis-thieno-[4″,5″-*b*″:4‴,5‴-*b*‴]silolo[2″,3″-*d*:2‴,3‴-*d*′]thiophene (ARSi) is a mutually fused structure hybridized with a BDT unit and two DTS units that share the two thiophene rings with the central BDT core. The ARSi moiety was copolymerized with naphtho[1,2-*c*:5,6-*c*′]bis[1,2,5]oxadiazole (NO) and 2,1,3-benzoxadiazole (BO) units to form alternating copolymers, PSiNO and PSiBO, respectively. The NO acceptor moiety is a symmetrical molecule composed of two BO units, providing a strong electron withdrawing character and affording better planarity to increase π-conjugation, which enhances close inter- and intramolecular interactions. At the same time, six solubilizing alkyl side-chains for every repeat unit in the ladder-type ARSi can be easily introduced onto the polymer backbone, which could improve the solution processing of the target polymers. We present a low bandgap copolymer PSiNO with a high molecular weight that performs well in BHJ inverted solar cells, affording a remarkable power conversion efficiency (PCE) of 8.37% along with a high open-circuit voltage (V_{oc}) of 0.90 V and a fill factor (FF) of 70.2% when blended with $PC_{71}BM$.

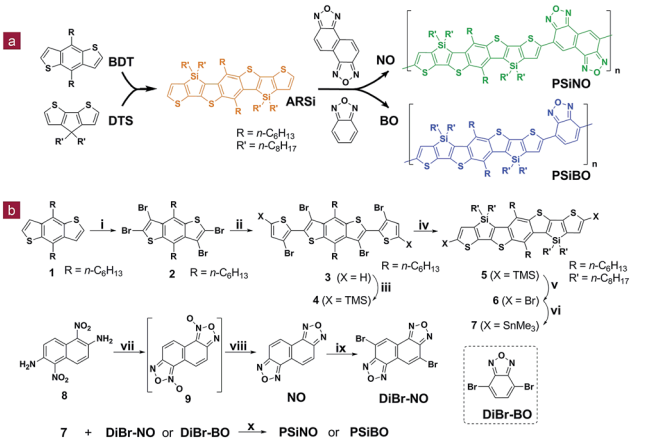

Scheme 1 (a) Schematic illustration of the procedure for the preparation of PSiNO and PSiBO copolymers. (b) Synthetic routes of the monomers and polymers. Reagents and conditions: (i) Br_2, $CHCl_3$/CH_3COOH (v/v = 2 : 1), rt then reflux. (ii) (3-bromothiophen-2-yl)-zinc chloride, $Pd(PPh_3)_4$, THF, reflux. (iii) (A) LDA, THF, −60 °C to rt; (B) TMSCl, −60 °C to rt. (iv) (A) *t*-BuLi, THF, −90 °C; (B) $Si(n\text{-}Oct)_2Cl_2$, −90 °C to rt. (v) NBS, THF, 0 °C. (vi) (A) *t*-BuLi, THF, −90 °C; (B) Me_3SnCl, −90 °C to rt. (vii) 1 M NaOH (95% EtOH), 5% NaClO (aq.), 0 °C. (viii) PPh_3, THF, reflux. (ix) NBS, CF_3COOH, H_2SO_4, 0 °C to rt. (x) $Pd_2(dba)_3$, $P(o\text{-tol})_3$, chlorobenzene.

The molecular weights (M_n) of the synthesized PSiNO and PSiBO polymers were determined by gel permeation chromatography (GPC) against polystyrene standards in a THF eluent and were found to be as high as 100.4 and 61.8 kDa, with polydispersity indices of 1.5 and 2.8, respectively. A high molecular weight is desirable because it improves the film formation and photovoltaic performance. Additionally, to ensure the solubility of the polymer, we adapted the polymer structure by incorporating six flexible aliphatic side-chains into the ARSi unit.

The thermal properties of the polymers were determined by thermogravimetric analysis (TGA) under a nitrogen atmosphere at a heating rate of 10 °C min^{-1} (Fig. S3†). Both polymers were

Scheme 1 outlines the chemical structure and synthetic route for the two copolymers by Stille cross-coupling reactions under microwave heating conditions. The starting material for the donor ARSi unit was 4,8-dihexylbenzo[1,2-*b*:4,5-*b*′]dithiophene (**1**),[29] which has good solubility. Bromination of **1** with Br_2 gave 2,3,6,7-tetrabromo-4,8-dihexylbenzo[1,2-*b*:4,5-*b*′]-dithiophene (**2**). Selective Negishi coupling between **2** and (3-bromothiophen-2-yl)-zinc chloride afforded compound **3**. Subsequent protection of the free α-positions of **3** by trimethylsilyl (TMS) groups formed compound **4**. Lithiation of all four brominated positions of **4** and the subsequent ring-closing reaction with dichlorodioctylsilane produced TMS-modified ARSi (**5**). Displacement of the TMS groups in **5** by *N*-bromosuccinimide produced compound **6**. Finally, stannylation of **6** afforded distannylated monomer **7** ready for polymerization. Inspired by the well-known BO acceptor,[8] the fused derivative NO acceptor was synthesized from 1,5-dinitronaphthalene-2,6-diamine **8** by a two-step procedure. Oxidative cyclization of **8** with sodium hypochlorite yielded *N*-oxide **9**, which was reduced with triphenylphosphane. Bromination of NO with *N*-bromosuccinimide gave dibromo-derivative DiBr-NO. All products were fully characterized by spectroscopic methods (see ESI†). Furthermore, the chemical structures and the planarity of dibromo-ARSi (**6**) and NO were unambiguously confirmed by single-crystal X-ray diffraction (Fig. S1†). Finally, distannylated-ARSi **7** and DiBr-NO were copolymerized by Stille cross-coupling reactions under microwave heating conditions to obtain the PSiNO copolymer. We also synthesized the BO-based analogous PSiBO copolymer for comparison. Crude polymers were purified by Soxhlet extraction with methanol, hexane, and chloroform. The chloroform solution was concentrated and the product was reprecipitated in methanol to obtain the target copolymers as brown fibrous solids. The number-average molecular weights

thermally stable with onset decomposition temperatures with 5% weight loss (T_d) at above 380 °C. No obvious thermal transitions were identified in the differential scanning calorimetry (DSC) curves of the second heating and cooling runs because of the rigid backbone that limits the chain motion.

Fig. 1a shows the absorption spectra of two polymers in dilute *o*-DCB solution and as thin films. Both polymers exhibit three well-defined absorption bands in *o*-DCB solution and as thin films, which imply that these two polymers have ordered structures both in solution and as thin films. The short-wavelength absorption bands from 400 to 500 nm are assigned to a delocalized excitonic π–π* transition of the heptacyclic moieties, whereas the long-wavelength absorption bands with well-resolved vibronic levels in the range of 500 to 900 nm are assigned to intramolecular charge transfer (ICT) interactions from the donor to the acceptor unit of the polymer backbone. The 0–0 and 0–1 transitions of the PSiBO/PSiNO ICT bands are located at 685/745 nm and 631/682 nm (shoulder), respectively. It has been reported that the higher the magnitude of this vibronic peak, the more ordered the microstructure.[30] Thus, the sharp ICT bands in the absorption spectra indicate that both PSiBO and PSiNO are highly rigid because of the coplanar conjugated structures. The intensity ratio for the 0–0 to the 0–1 transition of PSiNO is higher than that of PSiBO. In addition, a second shoulder (0–2 transition) of the PSiNO ICT band that appears at ~600 nm is not visible in PSiBO. For molecules with no symmetry constraints, the higher intensity ratio indicates less change in the chromophoric bond distances upon Franck Condon excitation. For D–A polymers, it implies more extensive π-delocalization and hence a higher degree of coplanarity/rigidity. Indirectly, this result leads us to conclude that the acceptor strength of NO (PSiNO) is greater than that of BO (PSiBO). This viewpoint is supported by the optical bandgaps (E_g^{opt}) deduced from the absorption onsets of the film spectra, which are in the order of PSiBO (1.70 eV) > PSiNO (1.56 eV).

To gain more insight into the effect of planarization on the molecular structures and electronic properties, theoretical calculations with density functional theory (DFT) at the B3LYP/6-31G* level were performed on dimers with methyl-substituted alkyl chains for simplicity. Both truncated polymers have excellent planarity through the entirety of the polymer backbone (Fig. 1b). The torsion angles between the D–A repeat units are < 1.3°, implying that the polymer backbone of PSiNO and PSiBO are free of steric hindrance between adjacent D and A units, so that the coplanar conformation can be easily retained in solution and the solid state. The wave functions of the frontier molecular orbital are depicted in Fig. S4.† The electron density in the HOMO wave function is mostly delocalized along the whole polymer backbone, whereas the electron density associated with the LUMO is localized at the electron acceptor site. The good wave function

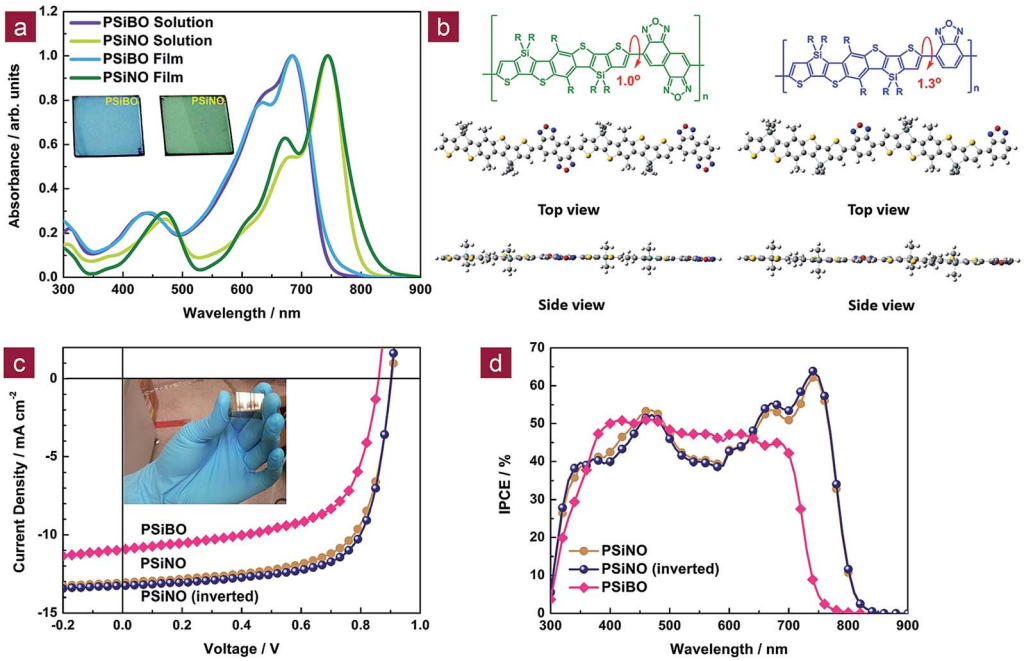

Fig. 1 (a) Normalized UV-vis absorption spectra of the target polymers in *o*-DCB solution and as thin films. Inset: photograph of PSiBO and PSiNO films (from left to right) showing variation in color. (b) Minimum energy conformations of PSiNO (left) and PSiBO (right) dimers with their calculated torsion angles. (c) *J*–*V* curves of optimized devices based on 1 : 1.5 PSiNO:$PC_{71}BM$ solar cells with 0.5 vol% DIO and 1 : 1 PSiBO:$PC_{71}BM$ solar cells with 3 vol% DIO under AM 1.5G solar illumination, and (d) corresponding IPCE spectra of optimized 1 : 1.5 PSiNO:$PC_{71}BM$ and 1 : 1 PSiBO:$PC_{71}BM$ devices illuminated with monochromatic light. Legend: light brown circles (●) represent the PSiNO conventional device (V_{oc} = 0.90 V, J_{sc} = −13.10 mA cm^{-2}, FF = 67.4%, and PCE = 7.95%), navy circles (●) represent the PSiNO inverted device (V_{oc} = 0.90 V, J_{sc} = −13.25 mA cm^{-2}, FF = 70.2%, and PCE = 8.37%) and pink diamonds (◆) represent the PSiBO conventional device (V_{oc} = 0.86 V, J_{sc} = −10.93 mA cm^{-2}, FF = 62.3%, and PCE = 5.86%).

delocalization and the coplanarity should facilitate both intra- and intermolecular charge transport.

Cyclic voltammetry (CV) was then employed to measure the onset redox potentials of the polymers (Fig. S5†). The HOMO/LUMO energies for PSiNO and PSiBO are −5.50/−3.73 and −5.46/−3.55 eV, respectively. The silole unit possesses a certain amount of electron-accepting ability, which in turn lowers the HOMO/LUMO energy levels of PSiNO and PSiBO polymers.[31] Compared with PSiNO, PSiBO showed higher lying HOMO/LUMO energy levels, implying that the electron-withdrawing ability of the BO fragment was weaker than that of the NO unit (*vide supra*). Because V_{oc} of the BHJ PSCs correlates closely with the difference between the LUMO energy level of the fullerene and the HOMO energy level of the donor polymer, a larger V_{oc} for NO-based PSCs was expected. The LUMO energy levels of these two polymers were located at −3.55 to −3.73 eV, providing sufficient driving force for charge separation and electron transfer without too much energy loss.

The hole mobility of PSiNO and PSiBO was measured by the space charge limit current (SCLC) method.[32] PSiNO had a high hole mobility of 1.2×10^{-3} cm^2 V^{-1} s^{-1}, which was around three times higher than that of PSiBO (4.3×10^{-4} cm^2 V^{-1} s^{-1}) (see Fig. S6†). This variation in device behavior was attributed to the change in the coplanarity of the polymer backbone caused by the introduction of different acceptors. We can conclude that the fused NO acceptor enhances the intrachain mobility because of the extended π-conjugation and larger steric hindrance compared with the nonfused BO acceptor. This improves the carrier collection efficiency and partly accounts for the higher fill factor (FF) and short-circuit current density (J_{sc}) values for PSiNO devices.

To characterize the photovoltaic properties of PSiNO and PSiBO, conventional BHJ PSCs with a device configuration of ITO/PEDOT:PSS (40 nm)/polymer:$PC_{71}BM$ (90–115 nm)/poly-[(9,9-dioctyl-2,7-fluorene)-alt-(9,9-bis(3′-(*N*,*N*-dimethylamino) propyl)-2,7-fluorene)] (PFN) (5 nm)/Ca (20 nm)/Al (100 nm) were prepared and examined under simulated 100 mW cm^{-2} AM 1.5G illumination. Incorporating a thin PFN cathode interlayer can produce an interfacial dipole, resulting in a reduced electron injection barrier and an increased built-in potential across the device.[14] The optimized $PC_{71}BM$ ratios of PSiNO and PSiBO for the active layers of the PSCs were 1 : 1.5 and 1 : 1, respectively. The polymer active layers of PSiNO and PSiBO were spin-coated from *o*-DCB solutions with 0.5% and 3% (v/v) 1,8-diiodooctane (DIO) as an additive,[33] respectively. We found that the optimum thickness of the active layers was 90–115 nm for all devices. The *J*–*V* curves and incident photon-to-current efficiencies (IPCE) of solar cells are shown in Fig. 1c and d. The device performance details are summarized in Table 1. In the optimized 1 : 1.5 PSiNO:$PC_{71}BM$ device with no further thermal annealing, the V_{oc} reached 0.90 V, with a J_{sc} of 13.10 mA cm^{-2} and a FF of 67.4%, offering a high PCE of 7.95%. Conversely, a device based on optimized 1 : 1 PSiBO:$PC_{71}BM$ had a moderate PCE of 5.86%, with a V_{oc} of 0.86 V, a J_{sc} of 10.93 mA cm^{-2} and a FF of 62.3%. Further increases in the fullerene ratio had a negative effect on both J_{sc} and FF, which decreased the PCE. As expected from the low-lying HOMO energy levels of the polymers, the trend in V_{oc} agrees well with the electrochemical potentials. Encouragingly, the inverted device configuration of ITO/ZnO (40 nm)/PFN (5 nm)/PSiNO:$PC_{71}BM$/MoO_3 (8 nm)/Ag (100 nm) leads to superior device performance compared with the conventional device architecture. The configuration had a V_{oc} of 0.90 V, a J_{sc} of 13.25 mA cm^{-2} and a FF of 70.2%, delivering an exceptional PCE of 8.37%, owing to the improved J_{sc} and FF. Both J_{sc} and FF of the PSiNO devices were much higher than those of the PSiBO devices, which could be attributed to various factors: the absorption strength of the active layer; optimal morphology with a suitable domain size of the active layer; and higher charge carrier mobility that can promote the exciton separation, charge transport, and enhanced charge collection efficiency.[34] To verify the accuracy of the photo *J*–*V* measurements, the IPCE spectra of the devices were measured under monochromatic light illumination (Fig. 1d). Compared with the absorption spectra of pristine polymers, the substantially broadened IPCE responses in the visible region can be attributed to both the intrinsic absorptions of the polymers and $PC_{71}BM$. The IPCE spectra correspond well to the absorption spectra of the blends (Fig. S8†), establishing a close correlation with the photocurrents. The integrated J_{sc} values from the IPCE spectra are 12.68, 12.73 and 10.40 mA cm^{-2} for conventional PSiNO, inverted PSiNO and conventional PSiBO devices, respectively. The J_{sc} values calculated from integration of the IPCE spectra are within a 5% error, which agrees well with those obtained from the *J*–*V* measurements, supporting the reliability of the photovoltaic measurement.

Table 1 Photovoltaic parameters of optimized solar cells

Polymer	Polymer : $PC_{71}BM$	V_{oc} (V)	J_{sc} (mA cm^{-2})	FF (%)	PCE[a] (%)
PSiNO	1 : 1	0.90	12.88	62.1	7.20 (6.94)
PSiNO	1 : 1.5	0.90	13.10	67.4	7.95 (7.76)
PSiNO[b]	1 : 1.5	0.90	13.25	70.2	8.37 (8.08)
PSiNO	1 : 2	0.88	11.65	58.3	5.98 (5.70)
PSiBO	1 : 1	0.86	10.93	62.3	5.86 (5.62)
PSiBO	1 : 1.5	0.86	10.38	60.1	5.37 (5.10)
PSiBO	1 : 2	0.84	9.18	55.4	4.27 (3.95)

[a] Average PCE of 10 optimized devices in parentheses. [b] Inverted device configuration of ITO/ZnO/PFN/PSiNO:$PC_{71}BM$/MoO_3/Ag.

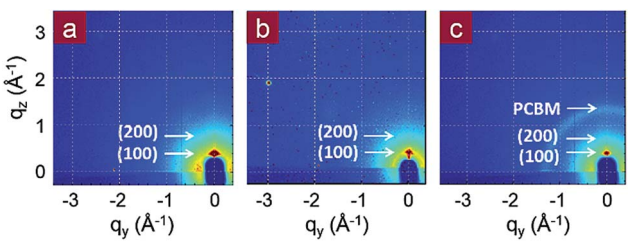

Fig. 2 Two-dimensional grazing incidence wide-angle X-ray scattering (GIWAXS) patterns of (a) PSiNO, (b) PSiBO neat films and (c) PSiNO:$PC_{71}BM$ (1 : 1.5) blend film.

To investigate the difference in the molecular packing and nanostructural order further, synchrotron grazing incidence wide-angle X-ray scattering (GIWAXS) analysis was performed to examine the neat polymer films and the optimized 1 : 1.5 PSiNO:$PC_{71}BM$ blend film. In Fig. 2a and b, both polymers show arc and anisotropic ring scattering patterns. The intensity of the (100) Bragg scattering peaks are strong at $q = 0.375$ Å^{-1} with an interlayer d_{100}-spacing of 16.8 Å for PSiNO and $q = 0.351$ Å^{-1} and an interlayer d_{100}-spacing of 17.9 Å for PSiBO, corresponding to the periodic lamellae of the polymer backbones. The weak diffraction peaks at $q = 0.753$ and 0.703 Å^{-1} for PSiNO and PSiBO, respectively, represent the second-order (200) reflections of lamellae (d_{200}-spacing = 8.34 and 8.94 Å). Furthermore, the stronger intensity of the (100) reflection in the out-of-plane scattering profile than in the in-plane scattering profile indicates that the lamellar packing of both polymers are preferentially stacked out of the film plane, although with some degree of randomness. The results can be attributed to the introduction of six flexible aliphatic side-chains into the ARSi unit, resulting in the misorientation of the polymer lamellae.[35] Nevertheless, the high degree of lamellar stacking is related to the planarity and rigidity of the polymer backbone, which enhances the intramolecular charge transport as well as the intermolecular charge transport parallel to the ITO substrate. The d_{100}-spacing of PSiNO was different from that of PSiBO by 1.1 Å, indicating that the NO unit offers more space to promote the close packing of alkyl side-chains interdigitating and tilting out of the polymer backbone plane in the solid state (Fig. S9†). Therefore, the PSiNO polymer chains are stacked more tightly than the PSiBO polymer chains. The net result is to affect intermolecular interactions and promote molecular packing. Additionally, a smaller *d*-spacing for PSiNO may facilitate the intermolecular charge transfer in high performance PSCs. The (010) reflections were almost undetectable, indicating poor π–π stacking of the polymer backbones owing to the out-of-plane side-chains that inhibit the order packing of the polymer backbones. In Fig. 2c, the $q = 1.4$ Å^{-1} halo is typical of amorphous scattering from the $PC_{71}BM$ aggregation within the blend, indicating random orientation with respect to the film substrate. Again, no clear π–π stacking reflection peak was observed, suggesting low crystallinity of the polymer blend. However, lamellar packing is still visible in the blends, indicating that PSiNO can maintain the same molecular arrangement when blended with fullerene. Therefore, the high hole mobility of the polymers does not result from the hopping of holes through an ordinary ordered π–π stacking route.[36–38] The novelty of this polymer lies in the high rigidity and planarity of its backbone, inhibiting the chain folding and extending the polymer chains. The extended chains allow charge carriers to percolate and be directly transported through the low-resistance polymer backbones, resulting in the high carrier mobility.

To gain a deeper insight into the effect of nanoscale morphology of the photoactive layers on PSCs, the morphological structures of both optimized blend films were analyzed by tapping-mode atomic force microscopy (TM-AFM) measurements.[39] The PSiNO and PSiBO blends displayed very different morphologies. Nanoscale fibril features were clearly visible in the PSiNO:$PC_{71}BM$ blend with a root mean square (RMS) roughness of 4.2 nm. The good phase separation is consistent with the more pronounced intermolecular stacking, as shown by the GIWAXS analysis (Fig. 3a). In contrast, the PSiBO:$PC_{71}BM$ blend showed unevenly aggregated polymer and $PC_{71}BM$ domains with a RMS roughness of 5.4 nm (Fig. 3b). This undesirable morphology may limit the exciton dissociation probability, resulting in exciton loss, geminate charge recombination, and poor charge mobility.[11,39] The well-ordered domains within the matrix, together with the high hole mobility of PSiNO, are likely to enable efficient charge separation and transport, which can explain the good performance of PSCs.

In conclusion, two low bandgap ladder-type copolymers of PSiNO and PSiBO that contain naphthobisoxadiazole (NO) and benzoxadiazole (BO) moieties, respectively, and silicon-bridged heptacyclic arene (ARSi) were designed and synthesized. Both polymers are highly rigid and coplanar, and have relatively low-lying HOMO energy levels that result in solar cells with a high open-circuit voltage. Both electron-donor ARSi and acceptor NO in this study are novel in terms of their synthetic chemistry and solar cell applications. On the one hand, the design strategy for ARSi is to provide three-in-one functionality: planarity, rigidity and charge transport efficiency. On the other hand, the strong electron-withdrawing ability of the NO moiety leads to stronger inter- and intra-chain interactions, higher charge carrier mobility, extends the absorption spectra toward the near IR region, and lowers the HOMO and LUMO energy levels and optical bandgap. For an inverted device structure, the maximum solar efficiency for PSiNO:$PC_{71}BM$ reaches 8.37% along with an open-circuit voltage of 0.90 V, a short-circuit current density of 13.25 mA cm^{-2} and a fill factor of 70.2% without thermal annealing, demonstrating that ARSi and NO moieties are a promising electron-donor/acceptor combination

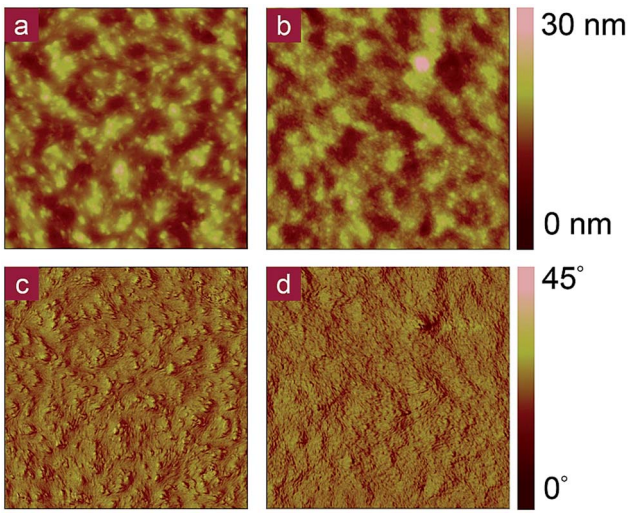

Fig. 3 Morphology characterization of TM-AFM topography images (upper row) and phase images (lower row) of 1 : 1.5 PSiNO:$PC_{71}BM$ blend films with 0.5 vol% DIO (panels a and c) and 1 : 1 PSiBO:$PC_{71}BM$ blend films with 3 vol% DIO (panels b and d). The image size is 3 × 3 μm for each panel.

for high-performance photovoltaics. More importantly, the high starting point of this device architecture, together with the low-ordering polymer framework, makes further improvement possible. Record performance could be achieved by integrating more efficient device architecture, such as ternary blends with small organic dyes, and plasmonic or microcavity architectures.

Acknowledgements

The devices fabrication was carried out in Advanced Laboratory of Accommodation and Research for Organic Photovoltaics, Ministry of Science and Technology of Taiwan. This work was also financially supported by the Ministry of Science and Technology of Taiwan.

Notes and references

1 B. Kippelen and J.-L. Brédas, *Energy Environ. Sci.*, 2009, **2**, 251.
2 S. C. Price, A. C. Stuart, L. Yang, H. Zhou and W. You, *J. Am. Chem. Soc.*, 2011, **133**, 4625.
3 C. E. Small, S. Chen, J. Subbiah, C. M. Amb, S.-W. Tsang, T.-H. Lai, J. R. Reynolds and F. So, *Nat. Photonics*, 2012, **6**, 115.
4 H.-C. Chen, Y.-H. Chen, C.-C. Liu, Y.-C. Chien, S.-W. Chou and P.-T. Chou, *Chem. Mater.*, 2012, **24**, 4766.
5 X. Guo, F. Liu, S. Zhang, L. Huo, T. P. Russell and J. Hou, *Adv. Mater.*, 2013, **25**, 4944.
6 I. Osaka, T. Kakara, N. Takemura, T. Koganezawa and K. Takimiya, *J. Am. Chem. Soc.*, 2013, **135**, 8834.
7 H.-C. Chen, Y.-H. Chen, C.-H. Liu, Y.-H. Hsu, Y.-C. Chien, W.-T. Chuang, C.-Y. Cheng, C.-L. Liu, S.-W. Chou, S.-H. Tung and P.-T. Chou, *Polym. Chem.*, 2013, **4**, 3411.
8 X. Wang, P. Jiang, Y. Chen, H. Luo, Z. Zhang, H. Wang, X. Li, G. Yu and Y. Li, *Macromolecules*, 2013, **46**, 4805.
9 S. B. Darling and F. You, *RSC Adv.*, 2013, **3**, 17633.
10 C. Cui, W.-Y. Wong and Y. Li, *Energy Environ. Sci.*, 2014, **7**, 2276.
11 H.-C. Chen, S.-W. Chou, W.-H. Tseng, I.-W. P. Chen, C.-C. Liu, C. Liu, C.-L. Liu, C.-h. Chen, C.-I. Wu and P.-T. Chou, *Adv. Funct. Mater.*, 2012, **22**, 3975.
12 X. Li, W. C. H. Choy, L. Huo, F. Xie, W. E. I. Sha, B. Ding, X. Guo, Y. Li, J. Hou, J. You and Y. Yang, *Adv. Mater.*, 2012, **24**, 3046.
13 Z.-G. Zhang, B. Qi, Z. Jin, D. Chi, Z. Qi, Y. Li and J. Wang, *Energy Environ. Sci.*, 2014, **7**, 1966.
14 Z. He, C. Zhong, X. Huang, W.-Y. Wong, H. Wu, L. Chen, S. Su and Y. Cao, *Adv. Mater.*, 2011, **23**, 4636.
15 C.-Z. Li, C.-Y. Chang, Y. Zang, H.-X. Ju, C.-C. Chueh, P.-W. Liang, N. Cho, D. S. Ginger and A. K.-Y. Jen, *Adv. Mater.*, 2014, **26**, 6262.
16 W. Cao and J. Xue, *Energy Environ. Sci.*, 2014, **7**, 2123.
17 Z. He, C. Zhong, S. Su, M. Xu, H. Wu and Y. Cao, *Nat. Photonics*, 2012, **6**, 591.
18 Y. Sun, C. J. Takacs, S. R. Cowan, J. H. Seo, X. Gong, A. Roy and A. J. Heeger, *Adv. Mater.*, 2011, **23**, 2226.
19 Z. Xu, L.-M. Chen, G. Yang, C.-H. Huang, J. Hou, Y. Wu, G. Li, C.-S. Hsu and Y. Yang, *Adv. Funct. Mater.*, 2009, **19**, 1227.
20 J. H. Seo, A. Gutacker, Y. Sun, H. Wu, F. Huang, Y. Cao, U. Scherf, A. J. Heeger and G. C. Bazan, *J. Am. Chem. Soc.*, 2011, **133**, 8416.
21 A. Kumar, G. Lakhwani, E. Elmalem, W. T. S. Huck, A. Rao, N. C. Greenham and R. H. Friend, *Energy Environ. Sci.*, 2014, **7**, 2227.
22 J. E. Anthony, *Chem. Rev.*, 2006, **106**, 5028.
23 C.-Y. Chang, Y.-J. Cheng, S.-H. Hung, J.-S. Wu, W.-S. Kao, C.-H. Lee and C.-S. Hsu, *Adv. Mater.*, 2012, **24**, 549.
24 Y.-X. Xu, C.-C. Chueh, H.-L. Yip, F.-Z. Ding, Y.-X. Li, C.-Z. Li, X. Li, W.-C. Chen and A. K.-Y. Jen, *Adv. Mater.*, 2012, **24**, 6356.
25 J.-S. Wu, S.-W. Cheng, Y.-J. Cheng and C.-S. Hsu, *Chem. Soc. Rev.*, 2015, DOI: 10.1039/c4cs00250d.
26 H.-Y. Chen, J. Hou, A. E. Hayden, H. Yang, K. N. Houk and Y. Yang, *Adv. Mater.*, 2010, **22**, 371.
27 M. C. Scharber, M. Koppe, J. Gao, F. Cordella, M. A. Loi, P. Denk, M. Morana, H.-J. Egelhaaf, K. Forberich, G. Dennler, R. Gaudiana, D. Waller, Z. Zhu, X. Shi and C. J. Brabec, *Adv. Mater.*, 2010, **22**, 367.
28 Y.-L. Chen, C.-Y. Chang, Y.-J. Cheng and C.-S. Hsu, *Chem. Mater.*, 2012, **24**, 4766.
29 H. Pan, Y. Li, Y. Wu, P. Liu, B. S. Ong, S. Zhu and G. Xu, *J. Am. Chem. Soc.*, 2007, **129**, 4112.
30 R. C. Coffin, J. Peet, J. Rogers and G. C. Bazan, *Nat. Chem.*, 2009, **1**, 657.
31 B. C. Schroeder, R. S. Ashraf, S. Thomas, A. J. P. White, L. Biniek, C. B. Nielsen, W. Zhang, Z. Huang, P. S. Tuladhar, S. E. Watkins, T. D. Anthopoulos, J. R. Durrant and I. McCulloch, *Chem. Commun.*, 2012, **48**, 7699.
32 V. D. Mihailetchi, H. Xie, B. de Boer, L. J. A. Koster and P. W. M. Blom, *Adv. Funct. Mater.*, 2006, **16**, 699.
33 H.-C. Liao, C.-C. Ho, C.-Y. Chang, M.-H. Jao, S. B. Darling and W.-F. Su, *Mater. Today*, 2013, **9**, 326.
34 Y. Liang, Y. Wu, D. Feng, S.-T. Tsai, H.-J. Son, G. Li and L. Yu, *J. Am. Chem. Soc.*, 2009, **131**, 56.
35 I. Osaka, R. Zhang, J. Liu, D.-M. Smilgies, T. Kowalewski and R. D. McCullough, *Chem. Mater.*, 2010, **22**, 4191.
36 H. Bronstein, D. S. Leem, R. Hamilton, P. Woebkenberg, S. King, W. Zhang, R. S. Ashraf, M. Heeney, T. D. Anthopoulos, J. de Mello and I. McCulloch, *Macromolecules*, 2011, **44**, 6649.
37 H. Bronstein, Z. Chen, R. S. Ashraf, W. Zhang, J. Du, J. R. Durrant, P. S. Tuladhar, K. Song, S. E. Watkins, Y. Geerts, M. M. Wienk, R. A. J. Janssen, T. Anthopoulos, H. Sirringhaus, M. Heeney and I. McCulloch, *J. Am. Chem. Soc.*, 2011, **133**, 3272.
38 X. Zhang, L. J. Richter, D. M. DeLongchamp, R. J. Kline, M. R. Hammond, I. McCulloch, M. Heeney, R. S. Ashraf, J. N. Smith, T. D. Anthopoulos, B. Schroeder, Y. H. Geerts, D. A. Fischer and M. F. Toney, *J. Am. Chem. Soc.*, 2011, **133**, 15073.
39 W. Chen, M. P. Nikiforov and S. B. Darling, *Energy Environ. Sci.*, 2012, **5**, 8045.